International Journal of Hydrogen Energy 56 (2024) 1249–1256

Contents lists available at ScienceDirect

International Journal of Hydrogen Energy

journal homepage: www.elsevier.com/locate/he

Improved performance of lanthanide-doped UIO-66/Nafion hybrid proton exchange membrane for water electrolyzer

Qiancan Wang [a,b], Dongchen Shen [a,b], Zhengkai Tu [a,b,*], Song Li [a,b,**]

[a] Department of New Energy and Science Engineering, School of Energy and Power Engineering, Huazhong University of Science and Technology, Wuhan, 430074, China
[b] China-EU Institute for Clean and Renewable Energy, Huazhong University of Science and Technology, Wuhan 430074, China

ARTICLE INFO

Keywords:
Metal-organic frameworks
Proton exchange membrane
Proton conductivity
Water electrolysis

ABSTRACT

Incorporating metal-organic frameworks (MOFs) especially the ones with protic functional groups into proton exchange membrane (PEM) can effectively improve its proton conductivity. Lanthanide MOFs (Ln-MOFs) have been recognized as more potential candidates exhibiting proton dissociation capability. However, the performance of PEM upon integrating Ln-MOFs in water electrolyzer has yet to be investigated. In this study, Nafion composites with different loadings of lanthanide Ce-UiO-66 were prepared, characterized and tested by comparing with the non-lanthanide Zr-UiO-66. It was revealed that the proton conductivity of Ce-UiO-66/Nafion composite membrane was higher than pristine Nafion and Zr-UiO-66/Nafion membrane, which was attributed to the fact that the Ce-UiO-66 doping contributed to the construction of the hydrogen-bonded network to enhance the proton conductivity. At 3 wt% Ce-UiO-66 doping, the proton conductivity of the composite membrane can reach 124.45 mS/cm, which is significantly improved by 17 % compared with Zr-UiO-66/Nafion. Such a trend is mainly contributed by the lower proton affinity and proton transfer capability of Ce atoms in Ce-UiO-66, and the higher number of water molecules around Ce atoms favors the reduced tortuosity of the proton conduction pathway in membranes. Single electrolytic cell tests demonstrated the enhancement of electrolysis efficiency upon Ce-UiO-66 doping was improved from 58.77 % to 65.37 % at a current density of 2 A cm^{-2}.

1. Introduction

Proton exchange membrane water electrolysis (PEMWE) driven by renewable power is one of the most promising hydrogen production technology owing to its low carbon footprint, high efficiency, quick response and high compatibility with intermittent renewable energy [1–4]. As the core component of the electrolyzer, proton exchange membrane (PEM) [5–7] plays the role of conducting protons, isolating gases and supporting catalysts, and its stability and proton conductivity directly affect the performance of the PEMWE. Currently, the commercialized perfluorosulfonic acid (PFSA) PEM membranes such as Nafion and Dow exhibit good mechanical properties and proton conductivity but high cost [8]. In order to further improve its stability and proton conductivity, many strategies such as crosslinking, hybridization and nanoparticle doping have been employed to modify PEM. It is found that nanoparticle doping can regulate the flexibility and hydrophilicity of the composite membrane polymer [9]. Conventional nanoparticles, such as SiO_2 [10] and TiO_2 [11,12], have been used as dopants in composite membranes, and it has been experimentally demonstrated that doping them into Nafion membranes improves the water absorption capacity [13]. However, the ultra-low proton conductivity of these inorganic nanoparticles causes a decreased proton conductivity of PEM.

Nevertheless, doping proton-conducting functional materials (e.g. hydroxide [14], covalent organic frameworks [15]) can significantly enhance the performance of PEM, among which, metal-organic frameworks (MOFs) [16,17] composed of metal clusters and organic ligands featured with high specific surface area, high porosity, adjustable pore structure and functional ligands have become promising candidates. The abundant functional ligands and pore structures of MOFs provide more opportunities for proton conduction. Many studies have reported that doping MOFs into PEM are beneficial to the proton conduction. Donnadio et al. [18] found that the proton conductivity of Nafion

* Corresponding author. Department of New Energy and Science Engineering, School of Energy and Power Engineering, Huazhong University of Science and Technology, Wuhan, 430074, China.
** Corresponding author. Department of New Energy and Science Engineering, School of Energy and Power Engineering, Huazhong University of Science and Technology, Wuhan, 430074, China.
E-mail addresses: tzklq@hust.edu.cn (Z. Tu), songli@hust.edu.cn (S. Li).

https://doi.org/10.1016/j.ijhydene.2023.12.288
Received 18 October 2023; Received in revised form 15 December 2023; Accepted 27 December 2023
Available online 3 January 2024

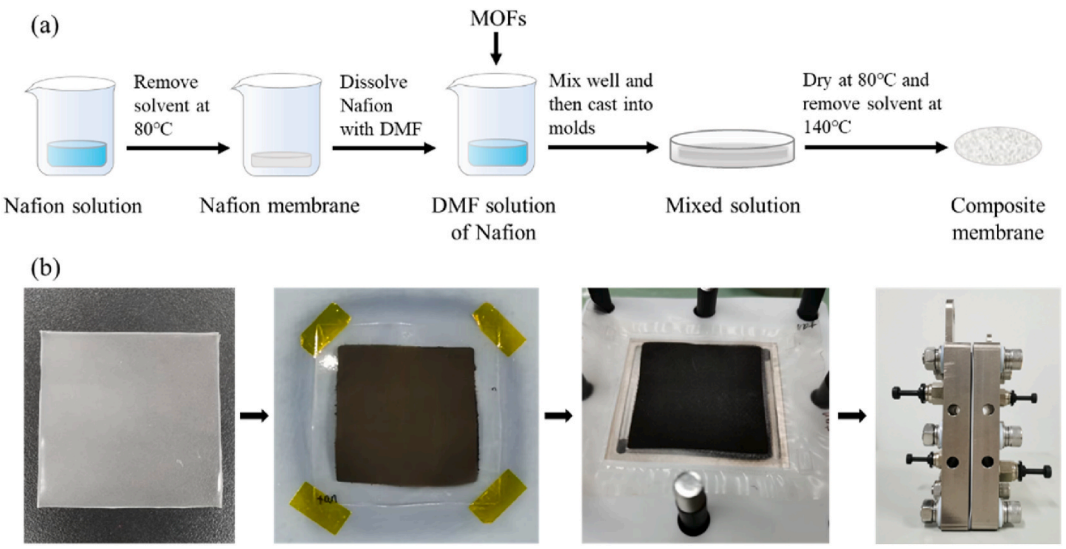

Fig. 1. (a) Schematic preparation process of the composite membrane; (b) preparation of membrane electrodes and assembly process of electrolyzer.

membranes doped with 2 wt% UiO-66 was increased by 30 % from 127 mS/cm to 165 mS/cm (at 80 °C, 95%RH), which was ascribed to the modified structural features that favors the proton transport. The composite membranes prepared with MIL-101(Cr) [19,20], MOF-801(Zr) [21], ZIF-8 [22] also exhibited enhanced proton conductivity, and their activation energies (E_a) were all decreased compared with pristine PEMs. This is probably due to the incorporation of MOFs contributing to the establishment of hydrogen-bonded networks in the PEM, which provide additional channels for proton transfer. The doping of MOFs also imposes a positive impact on the thermal stability of PEM [23,24]. It was found that the thermal stability of composite membranes were significantly improved after doping ZIF-8, and the desulfonation temperature increased from 340 to 360 °C, which was ascribed to the strong interaction between the imidazole ligand of ZIF-8 and the sulfonic acid group of the Nafion matrix [25].

Recently, the high proton conductivity of lanthanide MOFs (Ln-MOFs) has attracted growing attention [26]. A variety of Ln-MOFs were prepared to explore their applications in proton conduction, such as {H[$(N(CH_3)_4)_2$][Gd_3(NIPA)$_6$]}·3H_2O [27](71.2 mS/cm at 75 °C and 98% RH), {[Tb_4 (TTHA)$_2$ (H_2O)$_4$]·7H_2O}$_n$ [28](25.7 mS/cm at 60 °C and 98%RH), and ([Sm($H_5C_2P_2O_7$) (H_2O)$_2$]-TEG [29](91.7 mS/cm at 60 °C and 100%RH). It is revealed that lanthanide atoms of Ln-MOFs are prone to coordinate with water molecules at high coordination number, which facilitates the construction of hydrogen-bonded networks for proton conduction, endowing Ln-MOFs with excellent proton conductivity [26]. In addition, Ln-MOFs also exhibit outstanding water stability owing to the formation of stronger metal-ligand bonds in the presence of lanthanide atoms with higher charge densities, thus avoiding hydrolysis reactions [30]. The high proton conductivity and water stability enable Ln-MOFs potential PEM dopants. However, the proton conduction and hydrogen production performance of Ln-MOF doped PEM has yet to be elucidated.

In this work, in order to demonstrate the merits of Ln-MOFs for PEMWE, cerium-based UiO-66 (Ce-UiO-66) with mild synthesis conditions [31] and proton conduction potential [32] was chosen. For comparison, its non-lanthanide counterpart, i.e., zirconium-based UiO-66 (Zr-UiO-66) with high water stability [33] was also investigated. The two MOFs (i.e. Ce-UiO-66 and Zr-UiO-66) possess exactly identical topology and ligand except for the metal cluster. Both Ce-UiO-66 and Zr-UiO-66 of varying loadings were doped into Nafion. The prepared PEMs of Ce-UiO-66/Nafion and Zr-UiO-66/Nafion were characterized and tested, respectively. The microscopic mechanism of the improved proton conductivity of Ce-UiO-66/Nafion was further revealed by molecular simulations. The two membranes were also assembled into membrane electrode assembly (MEA) and tested in a PEM electrolyzer to assess their hydrogen production performance. In this work, we explored the proton conduction performance of two proton exchange membranes doped with Ce-UiO-66 and Zr-UiO-66, respectively, and revealed the mechanism of improved proton conduction of Ce-UiO-66/Nafion, which was further demonstrated by the enhanced water electrolysis performance.

2. Methodology

2.1. Materials

Cerium ammonium nitrate ($Ce(NH_4)_2(NO_3)_6$, analytically pure), acetic acid (CH_3COOH, analytically pure), N,N-dimethylformamide (DMF, analytically pure), anhydrous ethanol (CH_3CH_2OH, analytically pure), and acetone (CH_3OCH_3, analytically pure) were purchased from Shanghai Sinopharm Chemical Reagent Co. Zirconium chloride ($ZrCl_4$, 98 %, hafnium chloride ≤2 %), Nafion solution (D520CS, 5 wt%), acetonitrile (CH_3CN, chromatographic grade), terephthalic acid ($C_8H_6O_4$, 99 %) were purchased from Shanghai Aladdin Biochemical Technology Co. Iridium oxide catalyst (85 %) was purchased from Shaanxi Coal Industry Chemical Technology Research Institute Co. Platinum-carbon catalyst (60 % Pt) was purchased from Kunming Guiyan Catalyst Co. The deionized water was homemade in the laboratory. The above reagents were not treated before use.

2.2. Synthesis of Ce-UiO-66 and Zr-UiO-66

The preparation of Ce-UiO-66 was carried out according to the literature [34].180 ml acetonitrile and 5.32 g terephthalic acid were added to a round-bottomed flask, respectively followed by heating in an oil bath at 100 °C with thorough stirring. Then 60 ml aqueous solution of cerium ammonium nitrate (0.533 mol/L) were added to the flask and continued to stir at 100 °C for 2 h. After the mixture was cooled down to room temperature, the solids were separated by centrifugation, and then washed repeatedly with DMF and acetone. Finally, they were dried in an oven at 70 °C to obtain Ce-UiO-66.

Zr-UiO-66 was synthesized according to the literature [35]. First, 0.080 g (0.343 mmol) of $ZrCl_4$ and 30 equivalents of acetic acid (10.29 mmol) were dissolved in 20 ml of DMF and dispersed homogeneously by ultrasonication. 0.057 g (0.343 mmol) of terephthalic acid were added to the solution and stirred to dissolve. The mixture was poured into a

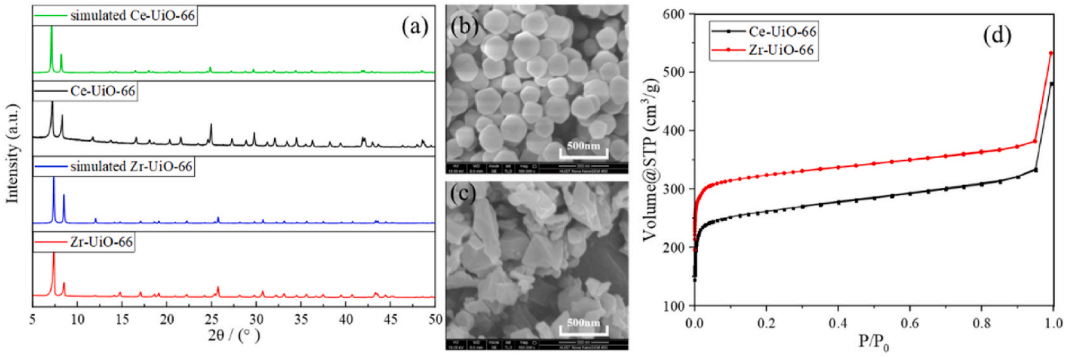

Fig. 2. (a) XRD patterns of Ce-UiO-66 and Zr-UiO-66; SEM images of (b) Ce-UiO-66, (c) Zr-UiO-66; (d) nitrogen adsorption isotherms of Ce-UiO-66 and Zr-UiO-66.

Teflon lined reactor and placed in an oven at 120 °C for 24 h. After the reactor was cooled to room temperature, the solid was separated by centrifugation and washed with ethanol. Zr-UiO-66 was obtained after vacuum drying.

2.3. Preparation of composite membranes and the membrane electrode assemblies

The composite membranes were prepared by casting method as demonstrated in Fig. 1. First, remove all solvents of Nafion solution at 80 °C and then add an equal amount of DMF to dissolve the resulting membrane to obtain Nafion solution with DMF as solvent. Ce-UiO-66 was dispersed in the Nafion solution in DMF by stirring and ultrasonication. The dispersion was poured into a mold, and heated up to 80 °C, then further dried in a vacuum oven at 140 °C to completely remove the solvents. Ce-UiO-66/Nafion membranes were named as Ce-*n*, where *n* presents the mass percentage of Ce-UiO-66 and $n = 1, 3, 5$. Similarly, Zr-UiO-66/Nafion membranes were named as Zr-1, Zr-3 and Zr-5, respectively. Membrane electrode assemblies (MEA) based on MOF/Nafion composite membrane were prepared by catalyst spraying method using automatic spray coating equipment (Anliu Tech. Co.). The activated area of MEA was 5×5 cm^2 and the catalyst loadings were 2 mg_{Ir}/cm^2 for the anode and 1 mg_{Pt}/cm^2 for the cathode, respectively. Titanium felts were used as the gas diffusion layer on both sides, and titanium bipolar plates with 1 mm fluid channels were employed.

2.4. Characterization

Powder X-ray diffraction (PXRD) was performed using an Empyrean instrument with a scanning range of $2\theta = 5°–50°$. Field Emission Scanning Electron Microscopy (SEM) was recorded with a Nova Nano-SEM 450. The FT-IR spectrum was obtained using Nicolet iS50R. The specific surface area and water vapor adsorption isotherms of the samples were obtained using a physical adsorption analyzer (Autosorb iQ2).

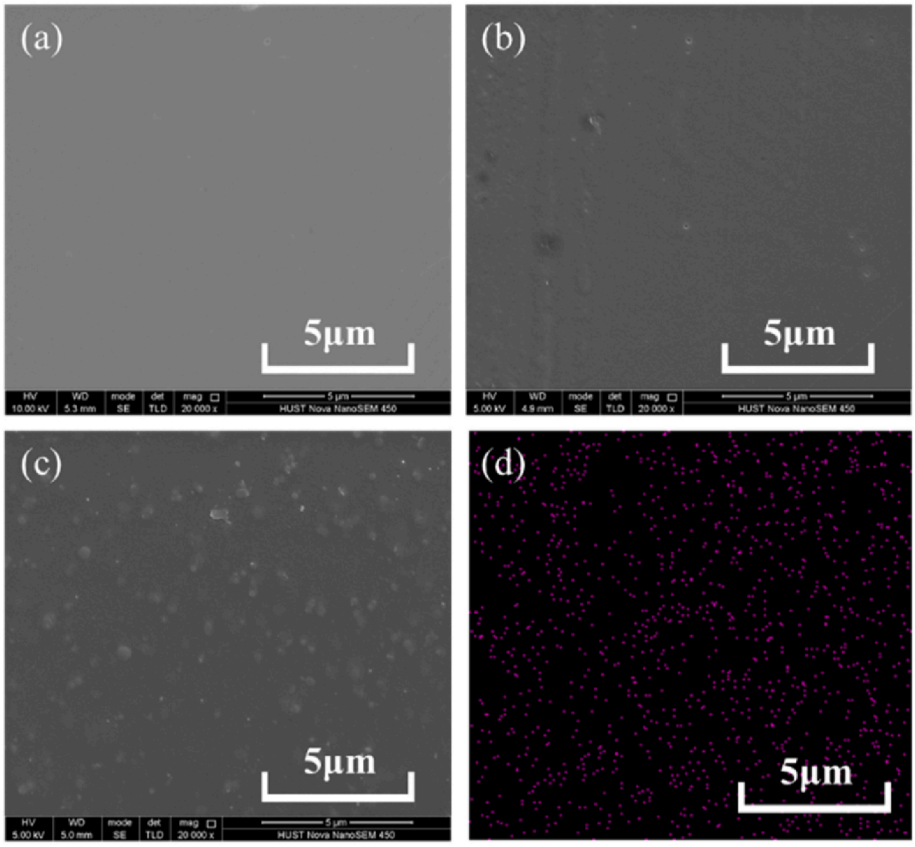

Fig. 3. SEM images of (a) Nafion, (b) Ce −3, (c) Zr −3; (d) distribution of Ce elements in Ce-3 from EDS.

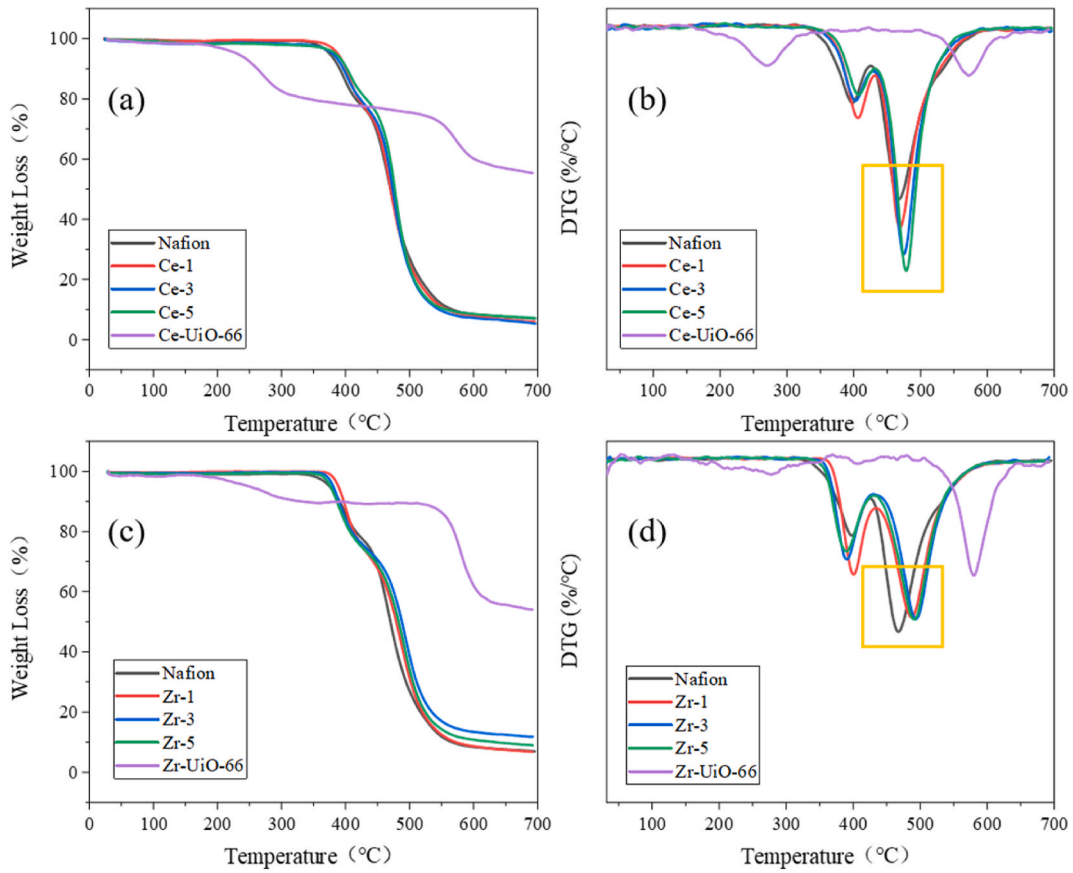

Fig. 4. TGA curves of (a) Ce-UiO-66 composite membranes and Ce-UiO-66; (b) Zr-UiO-66 composite membranes and Zr-UiO-66; DTG curves of (c) Ce-UiO-66 composite membranes and Ce-UiO-66; (d) Zr-UiO-66 composite membranes and Zr-UiO-66.

Thermogravimetric analysis was carried out on a Diamond thermogravimetric/differential thermal analysis (TG/DTA) using a heating rate of 20 °C/min under flowing nitrogen. The mechanical property was performed by electronic universal testing machine (CMT4104, Shenzhen Xinsansi Material Testing Co.). The water absorption and swelling test was performed at 80 °C to simulate the actual operating environment. The membrane was placed in ultrapure water and kept at 80 °C for 24 h to measure the changes in weight and size using electronic microbalance and optical microscope. The proton conductivity was tested by electrochemical impedance spectroscopy through CHI660E manufactured by Shanghai Chenhua Instrument Co. Ltd. with the frequency range of 1 MHz-1 Hz. The electrolyzer test was powered by a DC power supply, and the test was performed with a unilateral water supply to anode, with an inlet temperature of 80 °C at a flow rate of 25 ml/min.

2.5. GCMC simulations

The water adsorption behaviors of Ce-UiO-66 and Zr-UiO-66 were predicted by the lattice grand canonical Monte Carlo (GCMC) simulation [36]. Lennard-Jones (LJ) parameters of MOFs were derived from the universal force field (UFF) [37], and the atomic charges of MOFs were obtained from the density-derived electrostatic and chemical charge (DDEC) method by density functional theory [38] using VASP, while the force field parameters of Tip4p model [39] were utilized for water molecules. Considering the water-water interaction, the water molecules were described as the coarse-grained monatomic water (mW) water model [40], a single site interacting through anisotropic short-ranged potentials in lattice GCMC. 2×10^8 cycles were performed to obtain a convergence of the amount of adsorbed water, including 1×10^8 cycles for equilibration and 1×10^8 cycles for production.

For the sake of probing the distribution of water molecules in UiO-66, the radial distribution function (RDF, g(r)) between metal-water pairs was calculated by Ref. [41]:

$$g(r)\frac{V}{N_B}\frac{n_B}{4\pi r^2 dr}$$

where the n_B is the average number of particles at the distance between r and $r + dr$, while N_B and V represent the number of particles in the system and the total volume of the system, respectively.

3. Results and discussion

In order to validate the identity of the prepared Ce-UiO-66 and Zr-UiO-66, powder X-ray diffraction (PXRD) analysis was performed as shown in Fig. 2a. In the PXRD patterns, the characteristic peaks of Ce-UiO-66 and Zr-UiO-66 are in good agreement with the simulated results, indicating the good crystallinity and the successful synthesis of Ce-UiO-66 and Zr-UiO-66. The morphology of two MOFs from SEM in Fig. 2b–c demonstrate that Ce-UiO-66 exhibits relatively homogeneous polyhedral particles with diameter of 100–200 nm, which is consistent with literature [31]. Zr-UiO-66 exhibits a typical octahedral particle of about 200 nm [35]. Nitrogen adsorption test (Fig. 2d) showed that the specific surface area and total pore volume of Ce-UiO-66 are 1033.910 m^2/g and 0.497 cm^3/g ($P/P_0 = 0.90$), which are lower than those of Zr-UiO-66 (1295.340 m^2/g, 0.577 cm^3/g). Such a trend is in agreement with previous studies [34,35], which is possibly ascribed to the heavier atomic mass of Ce, leading to the reduced surface area per unit mass.

After doping with Nafion, almost no remarkable characteristic peaks of UiO-66 were observed in the XRD patterns of composite membranes (Fig. S1). The FT-IR spectra of composite membranes in Fig. S2 demonstrate no formation of chemical bond between UiO-66 and

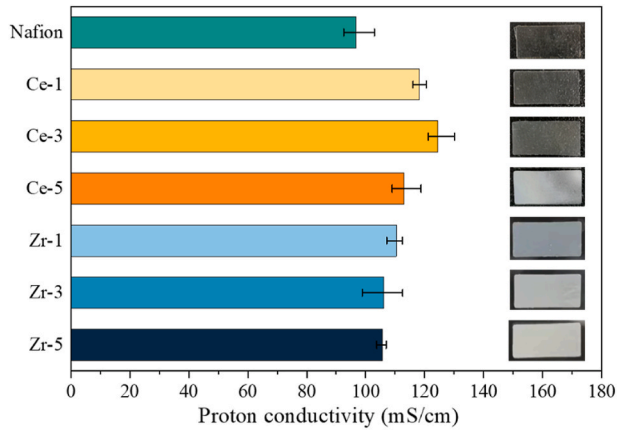

Fig. 5. Proton conductivity of Nafion and composite membranes at 80 °C and 90 %RH, and the photos of the corresponding membranes were on the right side.

Nafion, which is confirmed by XPS analysis (Fig. S3) The distribution of MOFs in the membrane was inspected by SEM. It is found that membrane surface was overall smooth without obvious ripples (Fig. 3). MOF particles in the Zr-UiO-66 doped membrane were uniformly dispersed (Fig. S4), and the amount increased significantly with the increase of the doping ratio. The Ce-UiO-66 doped composite membranes have similar surface morphology with Nafion, and it is difficult to directly observe the presence of Ce-UiO-66 (Fig. 3b) which is probably due to the smaller size of Ce-UiO-66 particles or its deep distribution in the membrane. Therefore, according to energy dispersive spectrum (EDS) in Fig. 3d, Ce elements of Ce-UiO-66 are uniformly distributed in the membrane, validating the well dispersion of Ce-UiO-66 particles in the composite membrane.

High thermal stability of doped PEM is a required for its application in electrolysis. TG-DTA analysis of Fig. 4 manifest that the composite membranes exhibit similar thermal stability with pristine Nafion membrane. The thermal degradation can mainly be divided into three steps [42]. At the temperature below 300 °C, the weight loss is mainly from the evaporation of water and residual solvent in the membrane. At the temperature of 300–420 °C, the weight loss is caused by the decomposition of sulfonate groups in the chain of Nafion. When the temperature increases above 420 °C, the backbone of Nafion began to decompose. The decomposition temperature of the Nafion backbone rises from 460 °C to 480 °C with increasing doping with Ce-UiO-66, and to 490 °C with Zr-UiO-66, indicating the improved thermal stability of composite membranes.

As the key evaluation criteria of PEM, proton conductivity was tested at 80 °C and 90 % RH to simulate the real working condition in the electrolyzer (Fig. 5). It is observed that all doped membranes exhibit higher proton conductivity than pristine one. Among all membranes, Ce-UiO-66 doped membrane at a loading of 3 wt% (Ce-3) exhibits the highest proton conductivity of 124.45 mS/cm, followed by the ones with the MOF loadings of 1 wt% and 5 wt%. In comparison, Zr-UiO-66 doped membrane at a loading of 1 wt% shows the highest proton conductivity of 110.42 mS/cm followed by the ones with MOF loadings of 3 wt% and 5 wt%. The proton conductivity of Ce-UiO-66 doped membrane was increased by 28 % compared with pristine Nafion. In previous studies, the enhanced proton conductivity of MOF doped membrane was commonly ascribed to its increased water uptake upon MOF doping, which favors the proton transfer via Vehicle mechanism owing to the formation of hydrogen-bonded network by more water molecules in the membranes [43,44]. On the contrary, the reduced water uptake of MOF

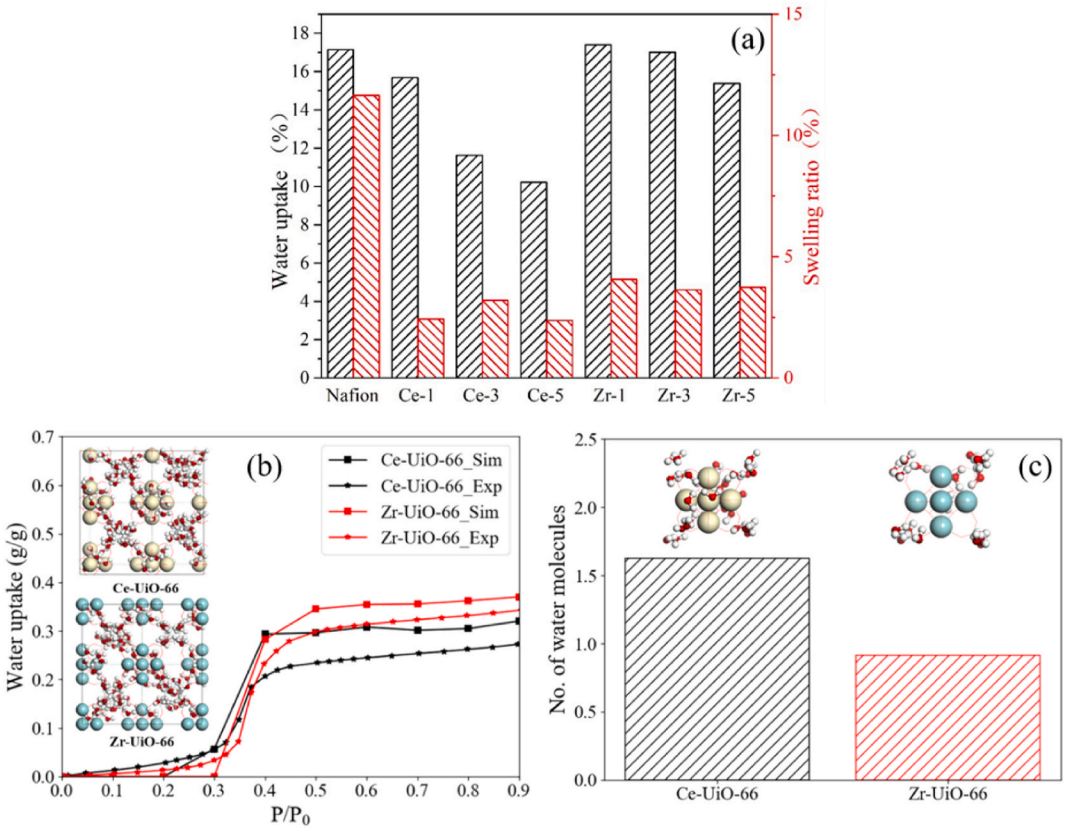

Fig. 6. (a) Gravimetric water uptake and swelling ratio of composite membranes; (b) Water adsorption isotherm and snapshots of UiO-66; (c) Number and snapshots of water molecules near metal. Zirconium (cyan), Cerium (yellow), Hydrogen (white), Oxygen (red), Carbon (gray). (For interpretation of the references to colour in this figure legend, the reader is referred to the Web version of this article.)

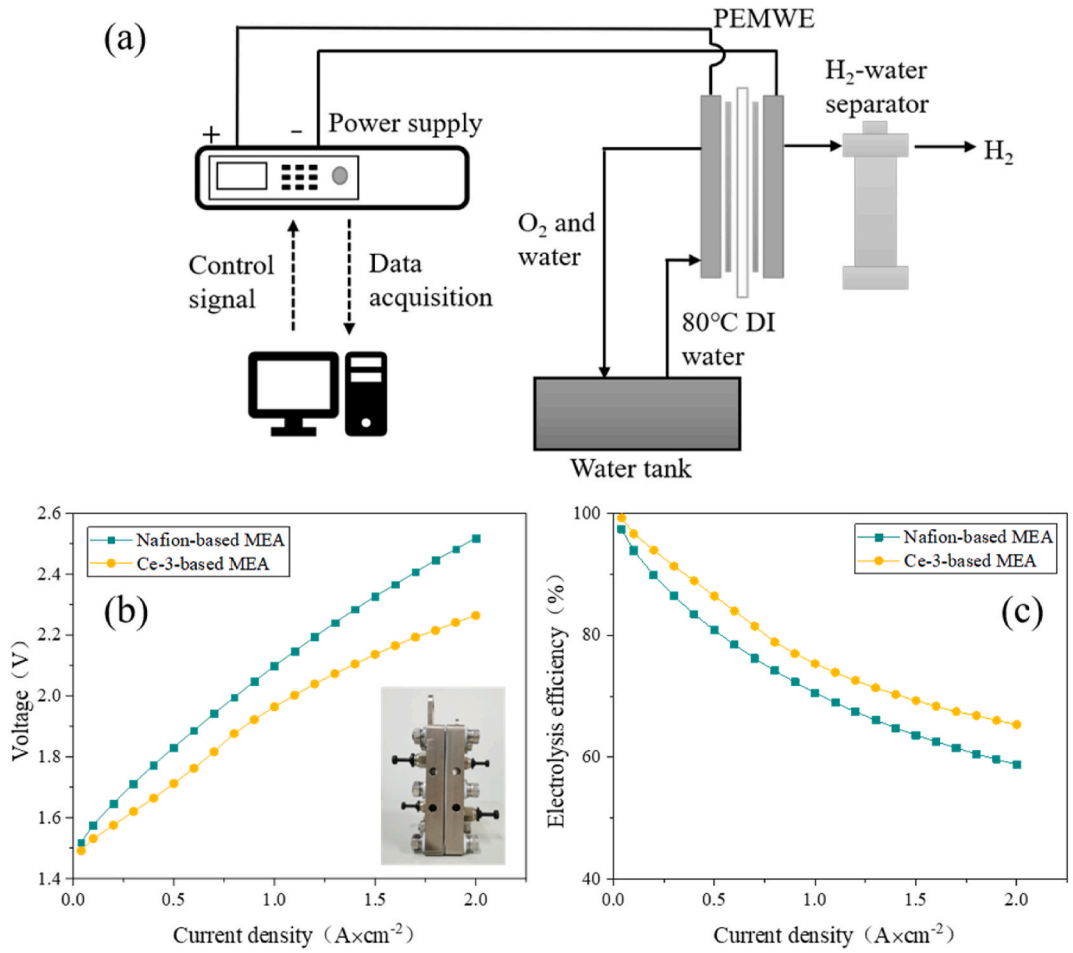

Fig. 7. (a) Schematic diagram of the test system of single-cell PEMWE; (b) the polarization curves of single-cell PEMWE based on MEA composed of pristine Nafion and Ce-3 membranes, (c) the electrolysis efficiency of single-cell PEMWE based on MEA composed of pristine Nafion and Ce-3 membranes.

doped membrane was also observed in Hf-MOF-801 doped Nafion membranes [21]. Nevertheless, the increased proton conductivity of the Hf-MOF-801 doped membrane was still observed, which may be due to the unsaturated sites and hydrophilic units in the MOF framework that contribute to the formation of hydrogen-bonded network.

In order to understand the mechanism of the enhanced proton conductivity of Ce-UiO-66 doped membrane in this work, the water uptake of the composite membranes was firstly tested at 80 °C (Fig. 6a). It is surprising that all the UiO-66 doped membranes exhibit lower water uptake than pristine Nafion membrane, indicating that the doped UiO-66 is not beneficial for the water uptake of composite membranes. Moreover, the water uptakes of Ce-UiO-66 doped membranes is generally lower than Zr-UiO-66 doped ones, which may be ascribed to the lower water adsorption capacity of Ce-UiO-66 at high humidity from experiments (Fig. 6b). Besides, the larger atomic mass of Ce than Zr is also contributed to the decreased water uptake percentage of Ce-UiO-66 doped membranes. In addition, the overall water uptakes of hybrid membranes decrease with the increased MOF loading, which may be mainly contributed by the fact that the increased weight from absorbed water is lower than that from doped MOFs. In the other hand, the swelling ratios of hybrid membranes are significantly reduced compared with the pristine Nafion, similar to previous report [45], in which it was ascribed to the reduces the free volume of membrane owing to the interaction between UiO-66 and Nafion. Besides, the rigidity of UiO-66 may impose constraints on the swelling behaviors of Nafion as well.

Regardless of the decreased water uptakes, the proton conductivity of the composite membranes was improved upon UiO-66 loading, to further explore such a phenomenon, GCMC simulations were performed to investigate the water adsorption behaviors of Ce-UiO-66 and Zr-UiO-66 (Fig. 6b). GCMC simulations demonstrates the lower water uptake of Ce-UiO-66 than Zr-UiO-66, which may be ascribed to the lower surface area and pore volume of Ce-UiO-66 that restricts its water uptake. Nevertheless, Ce-UiO-66 doped membranes exhibit higher proton conductivity than Zr-UiO-66 doped ones. Density functional theory calculations in previous work have shown that the proton affinity of Ce node is significantly lower than Zr node, indicating that the presence of Ce atoms facilitates the release of proton from its hydroxyl group, thus favoring proton conduction [46]. The average number of water molecules surrounding Ce and Zr atoms of UiO-66 obtained by RDF from GCMC simulations (Fig. 6c) revealed that the number of water molecules surrounding Ce is nearly twice of that nearby Zr, implicating the higher proton transfer capability of Ce nodes towards surrounding water molecules, directly improving the proton conductivity of membranes. Besides, the aggregated water molecules nearby Ce may favors the connectivity of proton conducting pathway and reduce its tortuosity [18].

Finally, the hydrogen production performance of MEA based on Ce-UiO-66 doped membrane was tested in electrolyzer (Fig. 7a) and compared with the one based on pristine Nafion. According to the polarization curves, the voltage of the electrolyzer based on MEA consisting of Ce-UiO-66 doped membrane is consistently lower, implicating its low electric resistance. At the low current density of 1 A cm^{-2}, the voltage of Ce-3-based MEA is 0.13 V higher than the one based on pristine Nafion. At the current density of 2 A cm^{-2}, the voltage difference of the two electrolyzers increases to 0.26 V. The electrolysis efficiency was further calculated based on the thermo-neutral voltage (V_{tn}

= 1.48 V) [47] according to the polarization curves. Generally, the electrolysis efficiency decreased with the current density. At the current density of 2 A cm^{-2}, the electrolysis efficiency of electrolyzer using Ce-3-based MEA is 65.37 %, which is 6.59 % higher than that of the electrolyzer using Nafion-based MEA. Such results demonstrate that the doping of Ce-UiO-66 effectively improves the proton conductivity of the membrane, which favors the reduction of the ohmic overpotential of the system, ultimately leading to improved electrolysis efficiency.

4. Conclusion

In this study, in order to investigate the effect of lanthanide-based MOF doping on the proton conductivity and hydrogen production performance of proton exchange membrane, Ce-UiO-66/Nafion and Zr-UiO-66/Nafion hybrid membrane at varying loadings were prepared, characterized and tested. It is revealed that UiO-66/Nafion hybrid membrane exhibited increased thermal stability, decreased swelling ratio and water uptakes compared with pristine membrane. Regardless of the lower water uptake, Ce-UiO-66/Nafion hybrid membrane exhibited significantly higher proton conductivity than Zr-UiO-66/Nafion. The proton conductivity of membrane with 3 wt% Ce-UiO-66 reached 124.45 mS/cm which is 28.63 % higher than Nafion. Based on the GCMC simulation, the enhanced proton conductivity can be ascribed to the lower proton affinity of Ce atoms that favors the proton dissociation of –OH groups. Besides, the increased number of water molecules surrounding Ce atoms compared with Zr also benefits the connectivity of proton transfer pathways in Ce-UiO-66/Nafion hybrid membrane. Moreover, the electrolysis efficiency of the electrolyzer using Ce-UiO-66/Nafion based MEA is increased by 6.59 % compared with pristine Nafion. This work provides insight into the mechanism of enhanced proton conductivity of Ln-MOF doped membrane and demonstrates the application potential of MOF/Nafion membrane for hydrogen production by water electrolyzer. It should be noted that although the proton conductivity of Ce-UiO-66/Nafion hybrid membrane reported in this work is not sufficiently high compared to other reported results. This work will inspire further exploration of high-performance Ln-MOF-doped PEM. In theory, Ln-MOFs with both high water uptake and high proton conductivity may endow PEM with better proton transfer performance, which requires investigation. Thus, the findings from this work may also provide guidelines to the development of high-performing Ln-MOFs based PEM for hydrogen production, and the mechanism of the improved proton conductivity may be extended to other Ln-MOFs based membranes.

Declaration of competing interest

The authors declare that they have no known competing financial interests or personal relationships that could have appeared to influence the work reported in this paper.

Appendix A. Supplementary data

Supplementary data to this article can be found online at https://doi.org/10.1016/j.ijhydene.2023.12.288.

References

[1] Carmo M, Fritz DL, Mergel J, Stolten D. A comprehensive review on PEM water electrolysis. Int J Hydrogen Energy 2013;38(12):4901–34.
[2] Zhang L, Zhao H, Xu S, Liu Q, Li T, Luo Y, Gao S, Shi X, Asiri AM, Sun X. Recent advances in 1D electrospun nanocatalysts for electrochemical water splitting. Small Structures 2021;2(2):2000048.
[3] Prabhu P, Do V-H, Peng CK, Hu H, Chen S-Y, Choi J-H, Lin Y-G, Lee J-M. Oxygen-bridged stabilization of single atomic W on Rh metallenes for robust and efficient pH-universal hydrogen evolution. ACS Nano 2023;17(11):10733–47.
[4] Nicole SLD, Li Y, Xie W, Wang G, Lee J-M. Heterointerface and tensile strain effects synergistically enhances overall water-splitting in Ru/RuO2 aerogels. Small 2023;19(10):2206844.
[5] Shirvanian P, Van Berkel F. Novel components in proton exchange membrane (PEM) water electrolyzers (PEMWE): status, challenges and future needs. A mini review[J]. Electrochemistry Communications 2020;114:106704.
[6] Wang X, Shao Z-G, Li G, Zhang L, Zhao Y, Lu W, Yi B. A cocrystallized catalyst-coated membrane with high performance for solid polymer electrolyte water electrolysis. J Power Sources 2013;240:525–9.
[7] Feng Q, Yuan X, Liu G, Wei B, Zhang Z, Li H, Wang H. A review of proton exchange membrane water electrolysis on degradation mechanisms and mitigation strategies. J Power Sources 2017;366:33–55.
[8] Ito H, Maeda T, Nakano A, Takenaka H. Properties of Nafion membranes under PEM water electrolysis conditions. Int J Hydrogen Energy 2011;36(17):10527–40.
[9] Tsai C-H, Wang C-C, Chang C-Y, Lin C-H, Chen-Yang YW. Enhancing performance of Nafion®-based PEMFC by 1-D channel metal-organic frameworks as PEM filler. Int J Hydrogen Energy 2014;39(28):15696–705.
[10] Adjemian KT, Srinivasan S, Benziger J, Bocarsly AB. Investigation of PEMFC operation above 100 °C employing perfluorosulfonic acid silicon oxide composite membranes. J Power Sources 2002;109(2):356–64.
[11] Santiago EI, Isidoro RA, Dresch MA, Matos BR, Linardi M, Fonseca FC. Nafion–TiO2 hybrid electrolytes for stable operation of PEM fuel cells at high temperature. Electrochim Acta 2009;54(16):4111–7.
[12] Ranganathan H, Vinothkannan M, Kim AR, Subramanian V, Oh M-S, Yoo DJ. Simultaneous improvement of power density and durability of sulfonated poly (ether ether ketone) membrane by embedding CeO2-ATiO2: a comprehensive study in low humidity proton exchange membrane fuel cells. Int J Energy Res 2022;46(7):9041–57.
[13] Vinothkannan M, Ramakrishnan S, Kim AR, Lee H-K, Yoo DJ. Ceria stabilized by titanium carbide as a sustainable filler in the nafion matrix improves the mechanical integrity, electrochemical durability, and hydrogen impermeability of proton-exchange membrane fuel cells: effects of the filler content. ACS Appl Mater Interfaces 2020;12(5):5704–16.
[14] Rehman MHU, Lufrano E, Simari C. Nanocomposite membranes for PEM-FCs: effect of LDH introduction on the physic-chemical performance of various polymer matrices. Polymers 2023;15(3):502.
[15] Meng X, Lv Y, Ding L, Peng L, Peng Q, Cong C, Ye H, Zhou Q. Effect of covalent organic frameworks containing different groups on properties of sulfonated poly (ether ether ketone) matrix proton exchange membranes. Nanomaterials 2022;12(19):3518.
[16] Ye Y, Gong L, Xiang S, Zhang Z, Chen B. Metal–organic frameworks as a versatile platform for proton conductors. Adv Mater 2020;32(21):1907090.
[17] Li X-M, Gao J. Recent advances of metal–organic frameworks-based proton exchange membranes in fuel cell applications. SusMat 2022;2(5):504–34.
[18] Donnadio A, Narducci R, Casciola M, Marmottini F, D'Amato R, Jazestani M, Chiniforoshan H, Costantino F. Mixed membrane matrices based on nafion/UiO-66/SO_3 H-UiO-66 nano-MOFs: revealing the effect of crystal size, sulfonation, and filler loading on the mechanical and conductivity properties. ACS Appl Mater Interfaces 2017;9(48):42239–46.
[19] Dong X-Y, Li J-J, Han Z, Duan P-G, Li L-K, Zang S-Q. Tuning the functional substituent group and guest of metal–organic frameworks in hybrid membranes for improved interface compatibility and proton conduction. J Mater Chem A 2017;5(7):3464–74.
[20] Li Z, He G, Zhao Y, Cao Y, Wu H, Li Y, Jiang Z. Enhanced proton conductivity of proton exchange membranes by incorporating sulfonated metal-organic frameworks. J Power Sources 2014;262:372–9.
[21] Ren H-M, Liu Y-R, Liu B-Y, Li Z-F, Li G. Comparative studies on the proton conductivities of hafnium-based metal–organic frameworks and related chitosan or nafion composite membranes. Inorg Chem 2022;61(25):9564–79.
[22] Barjola A, Escorihuela J, Andrio A, Giménez E, Compañ V. Enhanced conductivity of composite membranes based on sulfonated poly(ether ether ketone) (SPEEK) with zeolitic imidazolate frameworks (ZIFs). J Nanomater 2018;8(12):1042.
[23] Basu O, Das A, Jana T, Das SK. Design of flexible metal–organic framework-based superprotonic conductors and their fabrication with a polymer into proton exchange membranes. ACS Appl Energy Mater 2023;6(18):9092–107.
[24] Wu Y, Liu X, Yang F, Lee Zhou L, Yin B, Wang P, Wang L. Achieving high power density and excellent durability for high temperature proton exchange membrane fuel cells based on crosslinked branched polybenzimidazole and metal-organic frameworks. J Membr Sci 2021;630:119288.
[25] Wang L, Deng N, Wang G, Ju J, Wang M, Cheng B, Kang W. Construction of interpenetrating transport channels and compatible interfaces via a zeolitic imidazolate framework "bridge" for nanofibrous hybrid PEMs with enhanced proton conduction and methanol resistance. ACS Sustainable Chem Eng 2020;8(34):12976–89.
[26] Ren H-M, Wang H-W, Jiang Y-F, Tao Z-X, Mu C-Y, Li G. Proton conductive lanthanide-based metal–organic frameworks: synthesis strategies, structural features, and recent progress. Top Curr Chem 2022;380(2):9.
[27] Xing X-S, Fu Z-H, Zhang N-N, Yu X-Q, Wang M-S, Guo G-C. High proton conduction in an excellent water-stable gadolinium metal–organic framework. Chem Commun 2019;55(9):1241–4.
[28] Feng L, Wang H-S, Xu H-L, Huang W-T, Zeng T-Y, Cheng Q-R, Pan Z-Q, Zhou H. A water stable layered Tb(III) polycarboxylate with high proton conductivity over 10−2 S cm−1 in a wide temperature range. Chem Commun 2019;55(12):1762–5.
[29] Wang X, Lou D, Lu X, Wu J, Mu Y, Yan Y, Zhang Q, Bai M. Switching on the proton transport pathway of a lanthanide metal–organic framework by one-pot loading of tetraethylene glycol for high proton conduction. Dalton Trans 2018;47(27):9096–102.
[30] Wang C, Liu X, Demir NK, Chen JP, Li K. Applications of water stable metal–organic frameworks. Chem Soc Rev 2016;45(18):5107–34.

[31] Lammert M, Wharmby MT, Smolders S, Bueken B, Lieb A, Lomachenko KA, Vos DD, Stock N. Cerium-based metal organic frameworks with UiO-66 architecture: synthesis, properties and redox catalytic activity. Chem Commun 2015;51(63):12578–81.
[32] Bai Z, Wang Y, Liu W, Li Y, Xie J, Chen L, Sheng D, Diwu J, Chai Z, Wang S. Significant proton conductivity enhancement through rapid water-induced structural transformation from a cationic framework to a water-rich neutral chain. Cryst Growth Des 2017;17(7):3847–53.
[33] Gomes Silva C, Luz I, Llabrés I, Xamena FX, Corma A, García H. Water stable Zr–benzenedicarboxylate metal–organic frameworks as photocatalysts for hydrogen generation. Chem Eur J 2010;16(36):11133–8.
[34] Leubner S, Stäglich R, Franke J, Jacobsen J, Gosch J, Siegel R, Reinsch H, Maurin G, Senker J, Yot PG, Stock N. Solvent impact on the properties of benchmark metal–organic frameworks: acetonitrile-based synthesis of CAU-10, Ce-UiO-66, and Al-MIL-53. Chem Eur J 2020;26(17):3877–83.
[35] Schaate A, Roy P, Godt A, Lippke J, Waltz F, Wiebcke M, Behrens P. Modulated synthesis of Zr-based metal–organic frameworks: from nano to single crystals. Chem Eur J 2011;17(24):6643–51.
[36] Yu K, McDaniel JG, Schmidt JR. An efficient multi-scale lattice model approach to screening nano-porous adsorbents. J Chem Phys 2012;137(24):244102.
[37] Rappe AK, Casewit CJ, Colwell KS, Goddard WAI, Skiff WM. UFF, a full periodic table force field for molecular mechanics and molecular dynamics simulations. J Am Chem Soc 1992;114(25):10024–35.
[38] Manz TA, Limas NG. Introducing DDEC6 atomic population analysis: part 1. Charge partitioning theory and methodology. RSC Adv 2016;6(53):47771–801.
[39] Horn HW, Swope WC, Pitera JW, Madura JD, Dick TJ, Hura GL, Head-Gordon T. Development of an improved four-site water model for biomolecular simulations: TIP4P-Ew. J Chem Phys 2004;120(20):9665–78.
[40] Jacobson LC, Kirby RM, Molinero V. How short is too short for the interactions of a water potential? Exploring the parameter space of a coarse-grained water model using uncertainty quantification. J Phys Chem B 2014;118(28):8190–202.
[41] Jang SS, Molinero V, Çağın T, Goddard WA. Nanophase-segregation and transport in nafion 117 from molecular dynamics simulations: effect of monomeric sequence. J Phys Chem B 2004;108(10):3149–57.
[42] Zhu L, Li Y, Zhao J, Liu J, Wang L, Lei J, Xue R. Enhanced proton conductivity of Nafion membrane induced by incorporation of MOF-anchored 3D microspheres: a superior and promising membrane for fuel cell applications. Chem Commun 2022; 58(17):2906–9.
[43] Wang S. Amino acid-functionalized metal organic framework with excellent proton conductivity for proton exchange membranes[J]. Int J Hydrogen Energy: 11.
[44] Rao Z, Tang B, Wu P. Proton conductivity of proton exchange membrane synergistically promoted by different functionalized metal–organic frameworks. ACS Appl Mater Interfaces 2017;9(27):22597–603.
[45] Li Z, He G, Zhang B, Cao Y, Wu H, Jiang Z, Tiantian Z. Enhanced proton conductivity of nafion hybrid membrane under different humidities by incorporating metal–organic frameworks with high phytic acid loading. ACS Appl Mater Interfaces 2014;6(12):9799–807.
[46] Ho WH, Li S-C, Wang Y-C, Chang T-E, Chiang Y-T, Li Y-P, Kung C-W. Proton-conductive cerium-based metal–organic frameworks. ACS Appl Mater Interfaces 2021;13(46):55358–66.
[47] Selamet Ö F, Becerikli F, Mat MD, Kaplan Y. Development and testing of a highly efficient proton exchange membrane (PEM) electrolyzer stack. Int J Hydrogen Energy 2011;36(17):11480–7.